Lab on a Chip

CRITICAL REVIEW

View Article Online
View Journal | View Issue

Cite this: *Lab Chip*, 2017, **17**, 1689

Design and application of 'J-shaped' stress–strain behavior in stretchable electronics: a review

Yinji Ma,[ab] Xue Feng,[a] John A. Rogers,[c] Yonggang Huang[b] and Yihui Zhang *[a]

A variety of natural biological tissues (*e.g.*, skin, ligaments, spider silk, blood vessel) exhibit 'J-shaped' stress–strain behavior, thereby combining soft, compliant mechanics and large levels of stretchability, with a natural 'strain-limiting' mechanism to prevent damage from excessive strain. Synthetic materials with similar stress–strain behaviors have potential utility in many promising applications, such as tissue engineering (to reproduce the nonlinear mechanical properties of real biological tissues) and biomedical devices (to enable natural, comfortable integration of stretchable electronics with biological tissues/organs). Recent advances in this field encompass developments of novel material/structure concepts, fabrication approaches, and unique device applications. This review highlights five representative strategies, including designs that involve open network, wavy and wrinkled morphologies, helical layouts, kirigami and origami constructs, and textile formats. Discussions focus on the underlying ideas, the fabrication/assembly routes, and the microstructure–property relationships that are essential for optimization of the desired 'J-shaped' stress–strain responses. Demonstration applications provide examples of the use of these designs in deformable electronics and biomedical devices that offer soft, compliant mechanics but with inherent robustness against damage from excessive deformation. We conclude with some perspectives on challenges and opportunities for future research.

Received 18th March 2017,
Accepted 21st April 2017

DOI: 10.1039/c7lc00289k

rsc.li/loc

1. Introduction

Significant progress in the development of stretchable electronics[1–8] based on inorganic materials enables systems that combine extremely deformable mechanics and high-performance electrical properties. These unconventional technologies have significant commercial potential in biomedicine, either to replace the function of biological tissues/organs (*e.g.* skin-like prosthesis,[9–13] biomimetic robots,[14–17] *etc.*) or to integrate with biological tissues/organs (such as epidermal electronics,[18–24] flexible implantable medical instruments,[25–28] *etc.*).

[a] *Department of Engineering Mechanics, Center for Mechanics and Materials, AML, Tsinghua University, Beijing, 100084, China. E-mail: yihuizhang@tsinghua.edu.cn*
[b] *Departments of Civil and Environmental Engineering, Mechanical Engineering, and Materials Science and Engineering, Northwestern University, Evanston, IL 60208, USA*
[c] *Departments of Materials Science and Engineering, Biomedical Engineering, Chemistry, Mechanical Engineering, Electrical Engineering and Computer Science, Center for Bio-Integrated Electronics, Simpson Querrey Institute for Nano/Biotechnology, Northwestern University, Evanston, Illinois 60208, USA*

Yinji Ma

Yinji Ma is a postdoctoral fellow at the Northwestern University of USA. He received his PhD degree from Tsinghua University of China. His research interests include experimental mechanics, solid mechanics and flexible electronics.

Xue Feng

Xue Feng is a Professor of Engineering Mechanics at Tsinghua University. His research interests include flexible electronics, solid mechanics and experimental mechanics in extreme environments. He is an associate editor of "Journal of Applied Mechanics" (ASME Transactions), and serves on the editorial board of "npj Flexible Electronics" and "Flexible and Printed Electronics".

Many biological tissues, such as skin,[29,30] ligaments,[31] spider silk,[32,33] blood vessels,[34,35] *etc.*, exhibit 'J-shaped' stress–strain behaviors[36] as depicted in Fig. 1a,[29] as a result of their curved and chained microstructures (*e.g.*, collagen triple helix, collagen fibril, collagen fiber in Fig. 1a). This type of stress–strain response is typically characterized by three different stages. In stage I (Fig. 1a), wavy and crimped collagen fibers begin to unfurl by bending and twisting, thereby resulting in negligible stiffness and compliant mechanics (linear). As the applied strain increases (stage II), the collagen fibers uncoil, leading to an increase of the tangent modulus. After the collagen fibers straighten (stage III), the stress–strain behavior is dominated by stretching of the fibers, thereby offering a relatively linear response and a high tangent modulus. A goal in the development of engineering materials as substrates or superstrates in stretchable electronics focuses on the development of designs that can precisely reproduce the 'J-shaped' stress–strain behavior of real biological tissues.

To enable natural, comfortable integration of stretchable electronics with biological tissues/organs, an important design consideration is to reduce the stresses induced on the skin by the presence of the devices to within thresholds for somatosensory perception. Specifically, the electronics must be sufficiently compliant to accommodate deformations of soft biological tissues,[37,38] typically within several to tens of percent. Materials with 'J-shaped' stress–strain behavior are well-matched to this requirement due to their low elastic modulus at small strains.[39]

In the aforementioned applications, another challenge is in the development of materials/structures and strategies to minimize the possibility of mechanically induced device failure.[40–42] Several design concepts allow stretchable, integrated systems of hard, functional, inorganic components and soft, elastomeric substrates.[43–48] Here, an emerging design strategy involves the use of a layer with 'J-shaped' stress–strain behavior placed between the electronics and the biological tissue. This embedded layer has a high elastic modulus at large strain to shield the electronics from the potential for large deformations,[39,49] thereby providing a so-called "strain-limiting" function.

Fig. 1b–f summarize five structural designs that can offer 'J-shaped' stress–strain behavior: (i) network designs[49] that adopt wavy, horseshoe microstructures patterned in periodic lattices (*e.g.*, triangular, right-top; honeycomb, left-bottom; Kagome, right-bottom; Fig. 1b); (ii) wavy and wrinkled designs[50–53] induced using a pre-strain [unidirectional (top) or bidirectional (bottom) in Fig. 1c] strategy;

John A. Rogers

John A. Rogers is the Louis Simpson and Kimberly Querrey Professor of Materials Science and Engineering, Biomedical Engineering, Mechanical Engineering, Electrical Engineering and Computer Science, Chemistry and Neurological Surgery at Northwestern University where he also serves as Director of the Center on Bio-Integrated Electronics. Rogers' research focuses on unusual electronic and photonic devices, with an emphasis on bio-integrated and bio-inspired systems. He has published nearly 600 papers and is a member of the National Academy of Engineering, the National Academy of Sciences and the American Academy of Arts and Sciences.

Yonggang Huang

Yonggang Huang is the Walter P. Murphy Professor of Mechanical Engineering, Civil and Environmental Engineering, and Materials Science and Engineering at Northwestern University. He is interested in mechanics of stretchable and flexible electronics, and mechanically guided deterministic 3D assembly. He is a member of the US National Academy of Engineering. His recent research awards (since 2013) include the Drucker Medal in 2013, the Nadai Medal in 2016 from the American Society of Mechanical Engineers, and the Prager Medal in 2017 from the Society of Engineering Sciences; and he is listed as a Highly Cited Researcher.

Yihui Zhang

Yihui Zhang is an Associate Professor of Engineering Mechanics at Tsinghua University. Before joining Tsinghua, he was a Research Assistant Professor at Northwestern University. His research interests include mechanically guided 3D assembly, bio-inspired soft materials, and stretchable electronics. His recent honors and awards include the ASME Journal of Applied Mechanics Award (2017), MIT Technology Review's 35 Innovators Under 35 (2016), and Qiu Shi Outstanding Young Scholar Award (2016). He is an associate editor of Journal of Applied Mechanics (ASME Transactions), and serves on the editorial board of Proceedings of the Royal Society A, npj Flexible Electronics and Acta Mechanica Solida Sinica.

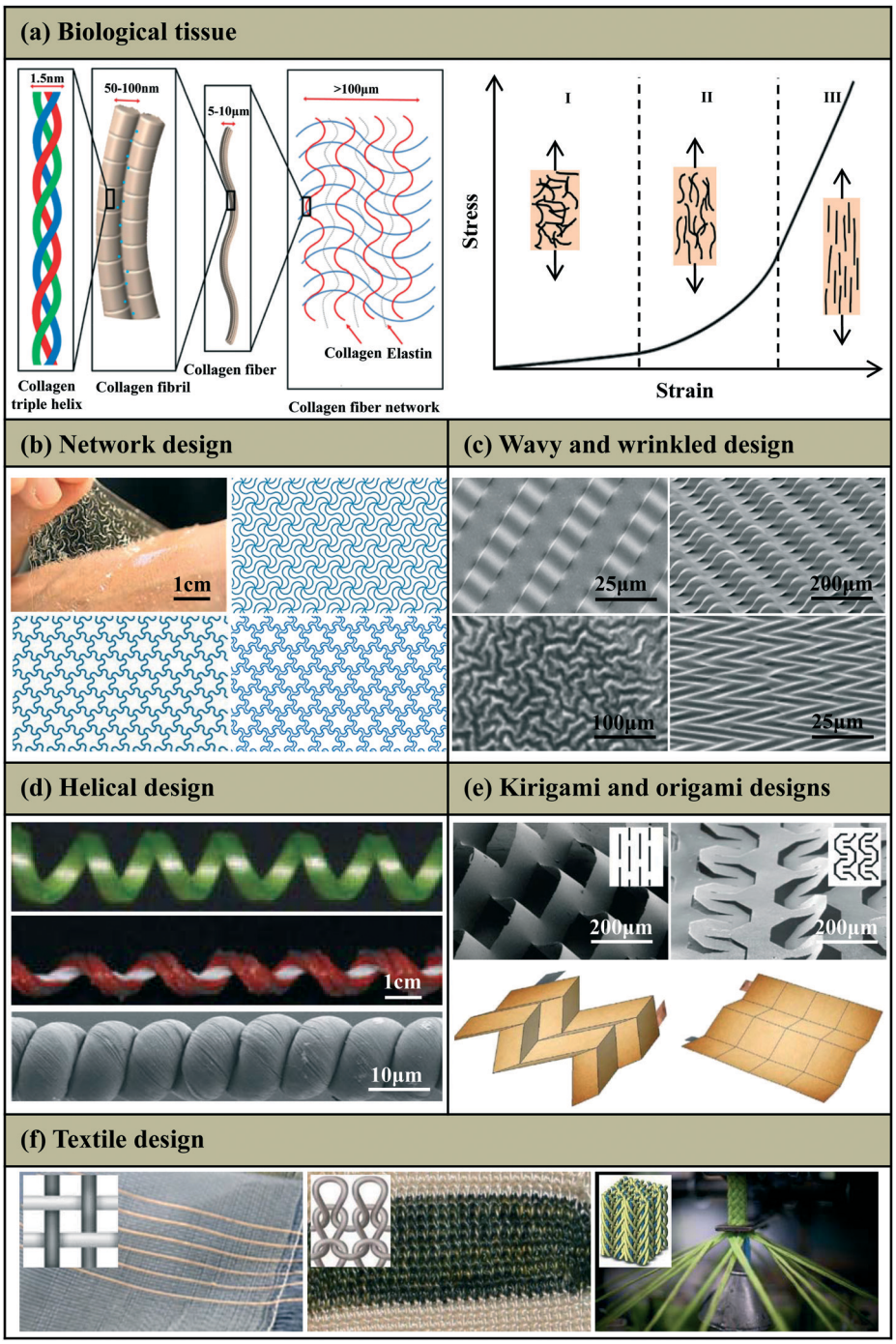

Fig. 1 Microstructures of biological tissues and five representative strategies to enable 'J-shaped' stress–strain behavior. (a) Hierarchical structure of a representative biological tissue spanning the nanoscale dimensions of collagen triple helices to microscale networks of collagen and elastin fibers, and its representative 'J-shaped' stress–strain behavior. (b) Network design: optical image (left-top) of a 2D network [triangular (right-top), honeycomb (left-bottom) and Kagome (right-bottom)] embedded in an ultralow-modulus matrix on skin. (c) Wavy and wrinkled design: stiff filamentary ribbons wrinkle on a unidirectionally pre-strained compliant substrate with uniform (left-top) and patterned (right-top) bonding, and stiff films wrinkle on an equi-biaxially (left-bottom) and nonequi-biaxially (right-bottom) pre-strained compliant substrate. (d) Helical design: coiled tendril, silicone fabric ribbon and helical carbon fiber. (e) Kirigami and origami designs: two microscale kirigami patterns in GO-PVA nanocomposites after photolithography (top) and quadrilateral mesh models and two representative Miura origami patterns (bottom). (f) Textile design: weaving (left), knitting (middle) and braiding (right). Panel (a) is adapted with permission from ref. 29 (Copyright 2015, Nature Publishing Group). Panel (b) is adapted with permission from ref. 49 (Copyright 2015, Nature Publishing Group). Panel (c) is adapted with permission from ref. 50 (Copyright 2006, the American Association for the Advancement of Science), ref. 51 (Copyright 2006, Nature Publishing Group), ref. 52 (Copyright 2015, John Wiley and Sons) and ref. 53 (Copyright 2007, American Chemical Society). Panel (d) is adapted with permission from ref. 54 (Copyright 2012, the American Association for the Advancement of Science) and ref. 55 (Copyright 2015, Nature Publishing Group). Panel (e) is adapted with permission from ref. 56 (Copyright 2015, Nature Publishing Group) and ref. 57 (Copyright 2014, Nature Publishing Group). Panel (f) is adapted with permission from ref. 58 (Copyright 2017, the American Association for the Advancement of Science) and ref. 59 (Copyright 2014, MDPI).

(iii) helical designs either with natural (*e.g.*, coiled tendril,[54] in the top of Fig. 1d) or synthetic (*e.g.*, silicone fabric ribbon[54] and helical carbon,[55] in the middle and bottom of Fig. 1d) constructions; (iv) kirigami (in the top of Fig. 1e)[56] and origami (in the bottom of Fig. 1e)[57] designs that exploit predefined patterns of cuts and creases; (v) textile designs manufactured by weaving (in the left of Fig. 1f),[58] knitting (in the middle of Fig. 1f)[58] or braiding (in the right of Fig. 1f)[59] to yield fabrics. Sections 2–6 summarize each design strategy, highlighting the fundamental principles as well as the key parameters that govern the 'J-shaped' stress–strain behavior. A brief discussion of the challenges and prospects for further study is presented in section 7.

2. Network design

Curved and chained microstructures in biological tissues (*e.g.*, collagen fiber network in Fig. 1a) consist of cross-linked fiber networks with random distributions[60–62] that can be reproduced, at some level, in synthetic materials by various approaches (*e.g.*, ionic liquid grinding,[63,64] two-step shearing,[65] plasma-induced modification[66] and two-step

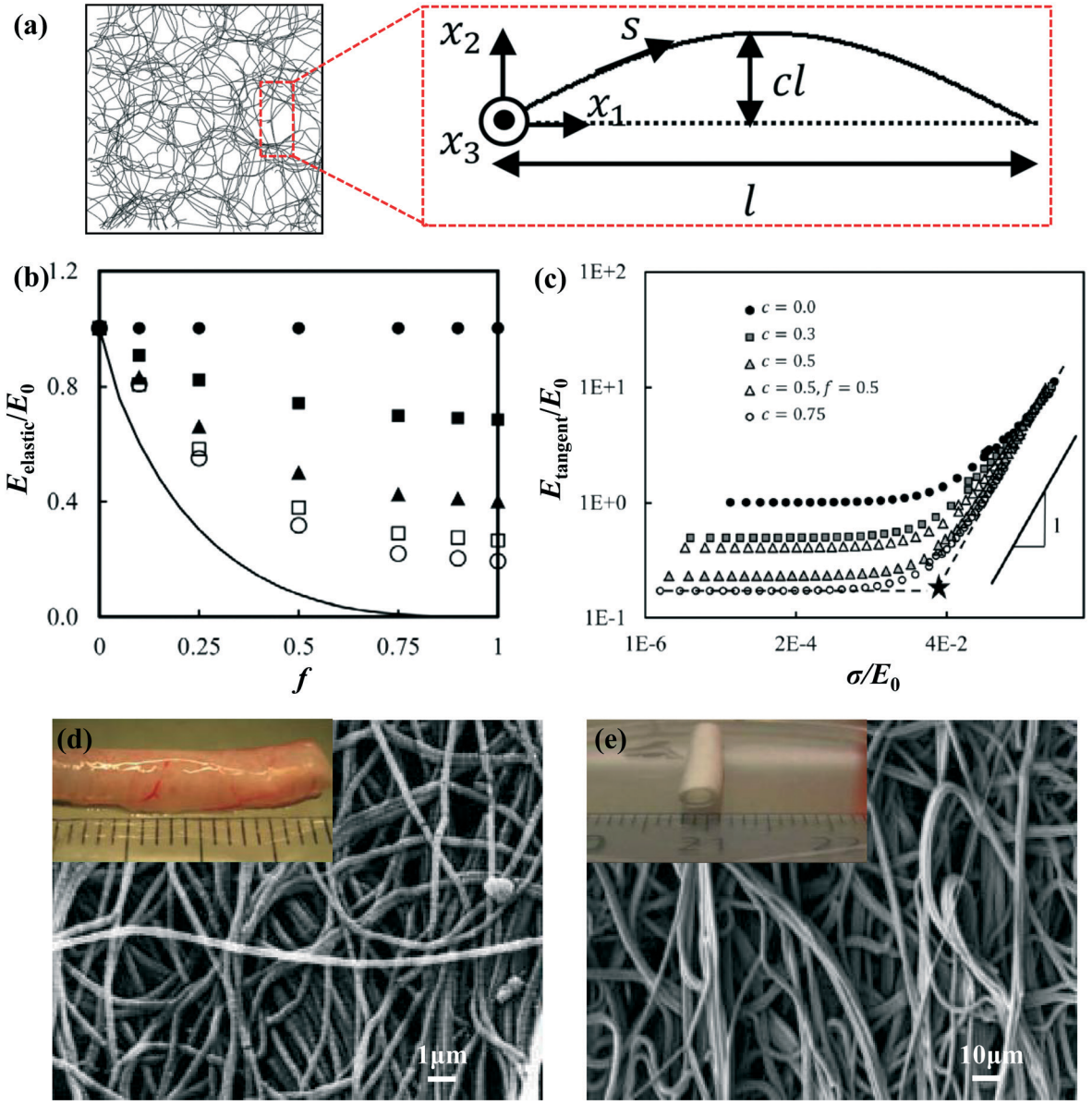

Fig. 2 Random network design. (a) Snapshot of an undeformed random network (f = 1 and c = 0.2) and schematic diagram of an individual crimped fiber. (b) Normalized network stiffness *versus* fraction of crimped fibers (f) with c = 0 (filled circles), 0.25 (filled squares), 0.5 (triangles), 0.66 (open squares), and 1 (open circles). The solid curve represents the lower bound of the normalized modulus stiffness ($E_{elastic}/E_0$). (c) Normalized tangent stiffness *versus* normalized true stress with f = 1 for all cases, except for that indicated in the legend. (d and e) SEM images of (d) native rat trachea and (e) electrospun artificial trachea (macroscopic view shown in inset figure). Panels (a)–(c) are adapted with permission from ref. 68 (Copyright 2016, ASME). Panels (d) and (e) are adapted with permission from ref. 69 (Copyright 2014, Nature Publishing Group).

polymerization[67]). Ban *et al.*[68] adopted a numerical approach to study the effect of fiber crimp on the stiffness of random fiber networks. To simulate the crimp, a fraction f of the total fibers are assumed to have a sinusoidal form with wavelength $2l$ and amplitude cl [*i.e.*, $x_2 = cl\sin(\pi x_1/l)$, as shown in Fig. 2a]. The other fibers are straight with length l. Fig. 2b shows that the normalized modulus stiffness [E_{elastic}/E_0, where E_{elastic} (f, c) is the elastic modulus at infinitesimal strain. $E_0 = E_{\text{elastic}}$ (f, 0)] decreases as f and c increase, indicating that the crimped fibers lead to a reduction of modulus. As the applied stress (σ) increases, the tangent modulus increases (Fig. 2c), due to the transition of deformations in the fibers from a bending to a stretching dominated mode. Jungebluth *et al.*[69] used electrospun synthetic fibers as artificial scaffolds, and then introduced cells to produce a tissue-engineered rat trachea (Fig. 2e) with microstructures and mechanical properties similar to those of native tissues (Fig. 2d). The percolation networks based on metal nanowires,[70,71] graphene flakes[72–74] and carbon nanotubes[75,76] have high conductivity, transmittance and magnetic response, and also can achieve the 'J-shaped' stress–strain behavior. The low modulus stages of such percolation networks due to the 'J-shaped' stress–strain behavior, together with their own physical characteristics, are well-matched with the demands of bio-integrated electronics.

Recent work establishes deterministic and bio-inspired design principles based on a two-dimensional (2D) wavy filamentary network embedded in an ultralow-modulus matrix. Here, the 'J-shaped' stress–strain behavior can be controlled, through careful choices in geometry, to precisely match those of human skin, as supported by finite element analyses (FEA) and experiments. Specifically, filamentary networks adopt a hierarchical construction of lattice topologies[77–83] with horseshoe microstructures,[46,84–88] as shown in Fig. 1b.[49] These microscale features can be formed in a variety of materials (*e.g.*, photodefinable polymers, metals and semiconductors) using lithographic approaches. Ma *et al.*[89] introduced a finite deformation model for horseshoe microstructures (inset, Fig. 3a) to predict the nonlinear stress–strain responses. Fig. 3a and b[89] show normalized stresses ($\sigma/E_{\text{material}}$) as a function of applied strain, where σ is the effective stress of the horseshoe microstructure, and E_{material} is the elastic modulus of the solid material. The resulting 'J-shaped' stress–strain behavior depends on two normalized parameters, the normalized width ($\bar{w} = w/R_0$) and the arc angle (θ_0). As the normalized width ($\bar{w}$) decreases, the transition of the 'J-shaped' stress–strain behavior becomes sharper, as shown in Fig. 3a. The critical strain for the transition between low and high modulus regimes is approximately $\varepsilon_{\text{cr}} = \theta_0/[2\sin(\theta_0/2)] - 1$, as marked by the dashed lines in Fig. 3a and b. A large arc angle (θ_0) gives a large critical strain, consistent with the results in Fig. 3b. As shown in Fig. 3c and d, the triangular lattice network (inset, Fig. 3c) maintains the 'J-shaped' stress–strain behavior of the horseshoe microstructures.[89] Four key parameters, the elastic modulus, transition strain, peak tangent modulus and peak strain, characterize the 'J-shaped' stress–strain curves of the lattice network. Quantitative mechanics models offer accurate predictions of these parameters as well as the deformed configurations.[89] Fractal designs[90] provide routes to strain-limiting materials with improved stretchabilities and multiple transition points during stretching. Fig. 3e shows the normalized stresses (in logarithmic scale) *versus* applied strain for first-, second- and third-order fractal horseshoe microstructures, respectively, with a fixed arc angle ($\theta_0 = 240°$), a normalized width ($\bar{w} = 0.2$) and 8 unit cells for each order. In addition, the high-order (*e.g.*, >2) fractal horseshoe microstructures have a substantially reduced elastic modulus, as compared to traditional, first-order horseshoe designs. This result is advantageous for strain-limiting materials in bio-integrated applications, due to reduced levels of induced stresses.

The network design can be implemented in a sandwich construction (Silbione/filamentary network/Silbione) to match precisely the non-linear stress–strain responses of human skin at different regions (*e.g.*, back and abdomen), as shown in Fig. 3f.[49] Here, a copper layer was deposited on a glass slide to serve as a sacrificial layer, followed by spin casting of a PI layer onto the top of the copper layer.[37] Photolithographic patterning of this PI layer enables formation of a deterministic network that was then transfer printed onto the surface of the elastomer, and uniformly coated with another elastomer layer. Transfer printing of the stretchable electronics onto this composite, strain-limiting structure finishes the integration of the entire device system. The strain-limiting effect of such network design can be also utilized to protect the electronics from levels of stretching that could lead to fracture of the electronic materials,[37] as shown in Fig. 3g.

3. Wavy and wrinkled design

For a stiff thin film bonded to a compliant substrate, differences in strain (either by thermally induced mismatch[91] or mechanical pre-strain[92–95]) between the film and substrate can lead to wrinkling of the film into a sinusoidal form (Fig. 1c). Fig. 4a presents a schematic illustration of a process for fabricating wavy films of PI bonded onto a low modulus silicone substrate (Silbione).[39] At small applied strain, the wrinkled PI film has negligible stiffness and does not contribute to the tensile stiffness of the system.[96] The result is a low elastic modulus (stage I in Fig. 4b), with a value that is almost the same as the intrinsic value of the substrate. As the applied strain increases, the wrinkled PI film becomes flat and therefore contributes to the stiffness of the system, yielding a high tangent modulus (stage II in Fig. 4b). As a result, the wrinkled film/substrate structure has a bilinear stress–strain behavior with an extremely sharp transition point, and an exceptionally high ratio of tangent to elastic modulus, which is particularly valuable as a strategy for constructing strain-limiting materials.

Release of the pre-strain in the substrate leads to the bending of the system with a curvature $\kappa H = 6[9\bar{E}_f h^3/\bar{E}_s H^3]^{1/3}$, when no additional constraints are involved.[96] If such

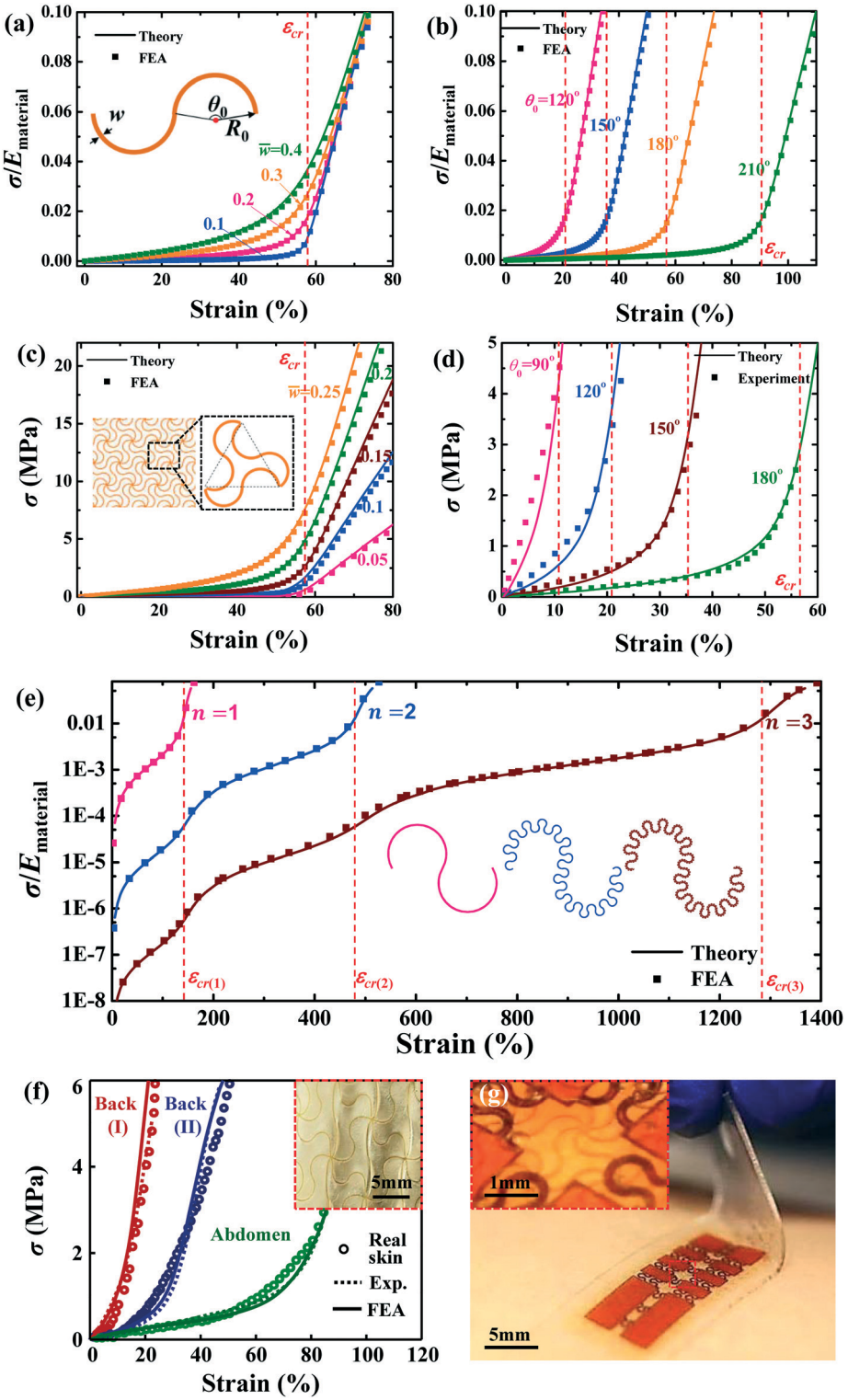

Fig. 3 Deterministic network design. Normalized stress–strain relation for a horseshoe microstructure with (a) a fixed arc angle (θ_0 = 180°) and several normalized widths ($\bar{w}$), and (b) a fixed normalized width ($\bar{w}$ = 0.2) & several arc angles (θ_0). Stress–strain relation for a network design based on a hierarchical triangular lattice consisting of horseshoe microstructures with (c) a fixed arc angle (θ_0 = 180°) & several normalized widths ($\bar{w}$), and (d) a fixed normalized width ($\bar{w}$ = 0.15) & several arc angles (θ_0). (e) Stress–strain relation for the first-, second- and third-order fractal horseshoe microstructures, respectively, with a fixed arc angle (θ_0 = 240°), a normalized width ($\bar{w}$ = 0.2) and 8 unit cells for each order. (f) Stress–strain responses of human skin and artificial skin at various locations on different individuals (inset figure: optical images of artificial skin). (g) Optical image of a core/shell structure with electronics that includes a strain-limiting layer in the form of a wave filamentary network of polyimide. Panels (a)–(d) are adapted with permission from ref. 89 (Copyright 2016, Elsevier). Panel (e) is adapted with permission from ref. 90 (Copyright 2016, ASME). Panel (f) is adapted with permission from ref. 49 (Copyright 2015, Nature Publishing Group). Panel (g) is adapted with permission from ref. 37 (Copyright 2015, John Wiley and Sons).

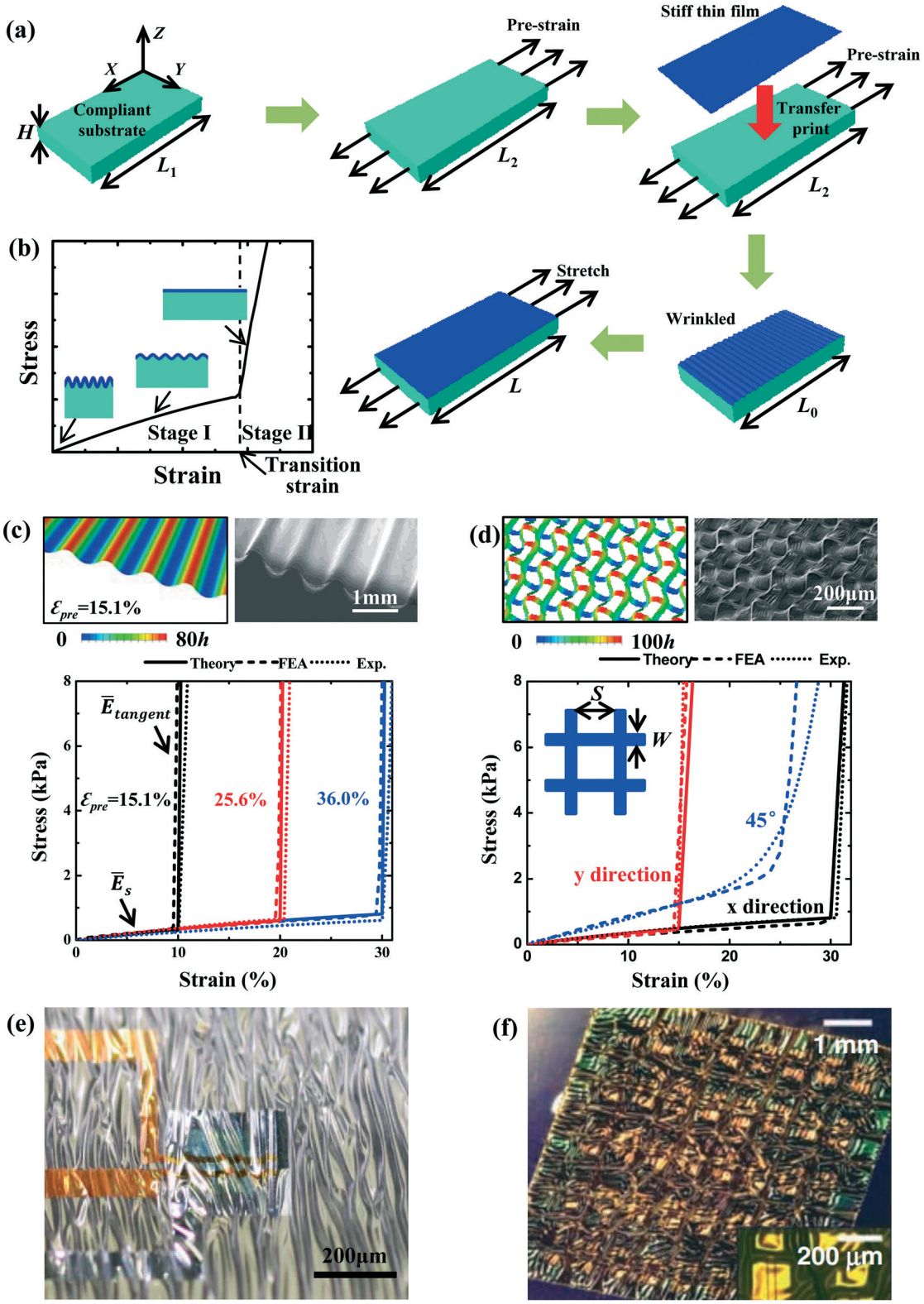

Fig. 4 Wavy and wrinkled design. (a) Schematic illustration of the process for fabricating wavy/wrinkled strain-limiting structures. (b) Bilinear stress–strain behavior of the strain-limiting structure. (c) Bilinear stress–strain curves of 1 μm-thick PI film on a 1 mm-thick Silbione substrate subjected to various pre-strains, along with its optical morphology and out-of-plane displacement subjected to 15.1% pre-strain. (d) Stress–strain curves for *x*-, *y*-, and 45°-stretching of a 1 μm-thick PI mesh (width W = 0.1 mm and spacing S = 0.4 mm) on a 1 mm-thick Silbione substrate subjected to pre-strains of ε^x_{pre} = 30.8% and ε^y_{pre} = 15.7%, along with its optical morphology and out-of-plane displacement. (e and f) Optical images of wrinkling electronic films when the substrate shrinks caused by (e) pre-strain releasing and (f) temperature change. Panels (a)–(d) are adapted with permission from ref. 39 (Copyright 2016, John Wiley and Sons). Panel (e) is adapted with permission from ref. 97 (Copyright 2013, Nature Publishing Group). Panel (f) is adapted with permission from ref. 98 (Copyright 2008, the American Association for the Advancement of Science).

bending is noticeable, it can be eliminated by adopting additional constraints, *e.g.*, through the use of fixtures to minimize the rotations of the system at two ends during the release of the pre-strain. When such a strain-limiting system sticks onto the target body (*e.g.*, skin), the bending can also be eliminated by applying constraints to the bottom surface of the system.

Substrates with finite thickness no longer recover to their initial length upon release of the pre-strain. The result is a transition strain ($\varepsilon_{transition}$, as shown in Fig. 4b) that is not equal to the pre-strain (ε_{pre}). Ma *et al.*[39] gives a relation between the transition strain ($\varepsilon_{transition}$) and the pre-strain (ε_{pre}) as

$$\varepsilon_{transition} = \frac{\varepsilon_{pre} - \frac{1}{4}\left(\frac{9\bar{E}_f h^3}{\bar{E}_s H^3}\right)^{1/3}}{1 + \frac{1}{4}\left(\frac{9\bar{E}_f h^3}{\bar{E}_s H^3}\right)^{1/3}}, \quad (1)$$

where H and h are the thicknesses of the substrate and the film, respectively. $\bar{E}_s = E_s/(1 - \nu_s^2)$ and $\bar{E}_f = E_f/(1 - \nu_f^2)$ are the plane-strain moduli of the substrate and the film, respectively, and E_s, E_f, ν_s and ν_f are the corresponding elastic moduli and Poisson's ratios. In addition to the transition strain, the ratio of the tangent to the elastic modulus also represents an important property, given by $\bar{E}_{tangent}/\bar{E}_{elastic} \approx 1 + \bar{h}E_f/(\bar{H}E_s)$.[39] Fig. 3c shows the bilinear stress–strain curves for a 1 μm-thick PI film on a 1 mm-thick Silbione substrate with three different levels of pre-strain.[39] The transition strains are 10%, 20% and 30%, respectively.

Fig. 4d shows a wavy, wrinkled design created by biaxial stretching. The thin film is replaced by a thin mesh (width $\bar{W}$ and spacing S, Fig. 4d) on a biaxially pre-strained (ε^x_{pre} and ε^y_{pre}), compliant substrate. The transition strain and ratio of tangent to elastic modulus are given by[39]

$$\varepsilon^i_{transition} = \frac{\varepsilon^i_{pre} - \frac{W}{6(W+S)}\left(\frac{9\bar{E}_f h^3}{\bar{E}_s H^3}\right)^{1/3}}{1 + \frac{W}{6(W+S)}\left(\frac{9\bar{E}_f h^3}{\bar{E}_s H^3}\right)^{1/3}}, \quad (2)$$

$$\frac{\bar{E}_{tangent}}{\bar{E}_{elastic}} \approx 1 + \left[W/(W+S)\right]\frac{\bar{E}_f h}{H\bar{E}_s}$$

where the superscript i denotes either x or y. Fig. 4d shows the stress–strain curves for x-, y- and 45°-stretching of a 1 μm-thick PI mesh on a 1 mm-thick Silbione substrate subjected to the pre-strains ε^x_{pre} = 30.8% and ε^y_{pre} = 15.7% (ref. 39). The resulting transition strains $\varepsilon^x_{transition}$ and $\varepsilon^y_{transition}$ are 30% and 15%, respectively.

In addition to 'J-shaped' stress–strain behavior, the wavy and wrinkled design also provides a route to stretchability in electronic materials, representing a strategy that has been widely used in many stretchable electronic devices. For example, Kaltenbrunner *et al.*[97] printed an ultrathin electronic polymer foil onto a pre-strained elastomer (Fig. 4e), which forms a wrinkled configuration that can accommodate relatively large tensile strains. Kim *et al.*[98] fabricated biaxially wavy CMOS (complementary metal-oxide semiconductor) circuits on a thin polymer film (Fig. 4f), through the use of biaxial thermal strain in the elastomeric substrate. Both of these examples[97,98] give a compliant response at small strain, due to the low elastic modulus. The polymer film becomes stiff when it is stretched flat again, which shields the electronics from high strains.

4. Helical design

Helical microstructures[99] also exhibit the 'J-shaped' stress–strain behavior.[100–104] For a helical ribbon, as shown in Fig. 5a, Pham *et al.*[105] gave an analytical expression that captures the non-linear mechanics response under the conditions that the ratio of $t/w \ll 11$ and $L/w \ll 1$, *i.e.*,

$$F = \frac{E\pi^2 w t^3 p}{3l^3}\left[\frac{\sqrt{1-(p_0/l)^2}}{\sqrt{1-(p/l)^2}} + \frac{1-\nu}{1+\nu}\right], \quad (3)$$

where the geometry is described by the contour length ($L = Nl$, with l denoting the contour length of a single turn, and N the number of helical turns), pitch (p), radius $\left(R = \sqrt{l^2 - p^2/2\pi}\right)$, width ($w$) and thickness ($t$), as illustrated in Fig. 5a. p_0 and R_0 are the initial pitch and radius. E and ν are the elastic modulus and Poisson's ratio of the material, respectively. To verify this analytical solution, Pham *et al.*[105] also carried out experiments on a helical carbon fiber (R_0 = 15 μm, L = 1190 μm, N = 12.5, w = 5.9 μm, t = 122 nm, E = 1.3 GPa and ν = 0.3). The measured force–displacement curves agree well with the analytical solution (eqn (3)), as shown in Fig. 5b.

Three-dimensional (3D) printing[99] (*e.g.*, fused deposition modeling,[106] UV-assisted 3D printing[107] and solvent-cast 3D printing[108]) represents one straightforward approach to helical microstructures, but with limited choices in materials. Fig. 5c summarizes an alternative strategy that uses mechanical assembly. Specifically, two strips of different lengths are adhered together side-by-side, after stretching the short strip to a length that matches that of the long one. Upon release of the stretch, this bi-strip twists and bends either into a helix or a hemihelix.[109–111] Recently, Xu *et al.*[112] reported a mechanically-guided approach for the assembly of complex, 3D architectures in a diversity of high-performance materials, including semiconductors (*e.g.*, silicon), metals (*e.g.*, Au, Cu, Ni), polymers (*e.g.*, PI, SU8), and their heterogeneous integration. Here, filamentary serpentine ribbons serve as 2D precursors that are bonded to a pre-stretched silicone elastomer at selected points (red dots in Fig. 5d). 3D helical microstructures form spontaneously upon release of the pre-strain. This type of 2D–3D geometric transformation follows from a process of compressive buckling that can be analyzed

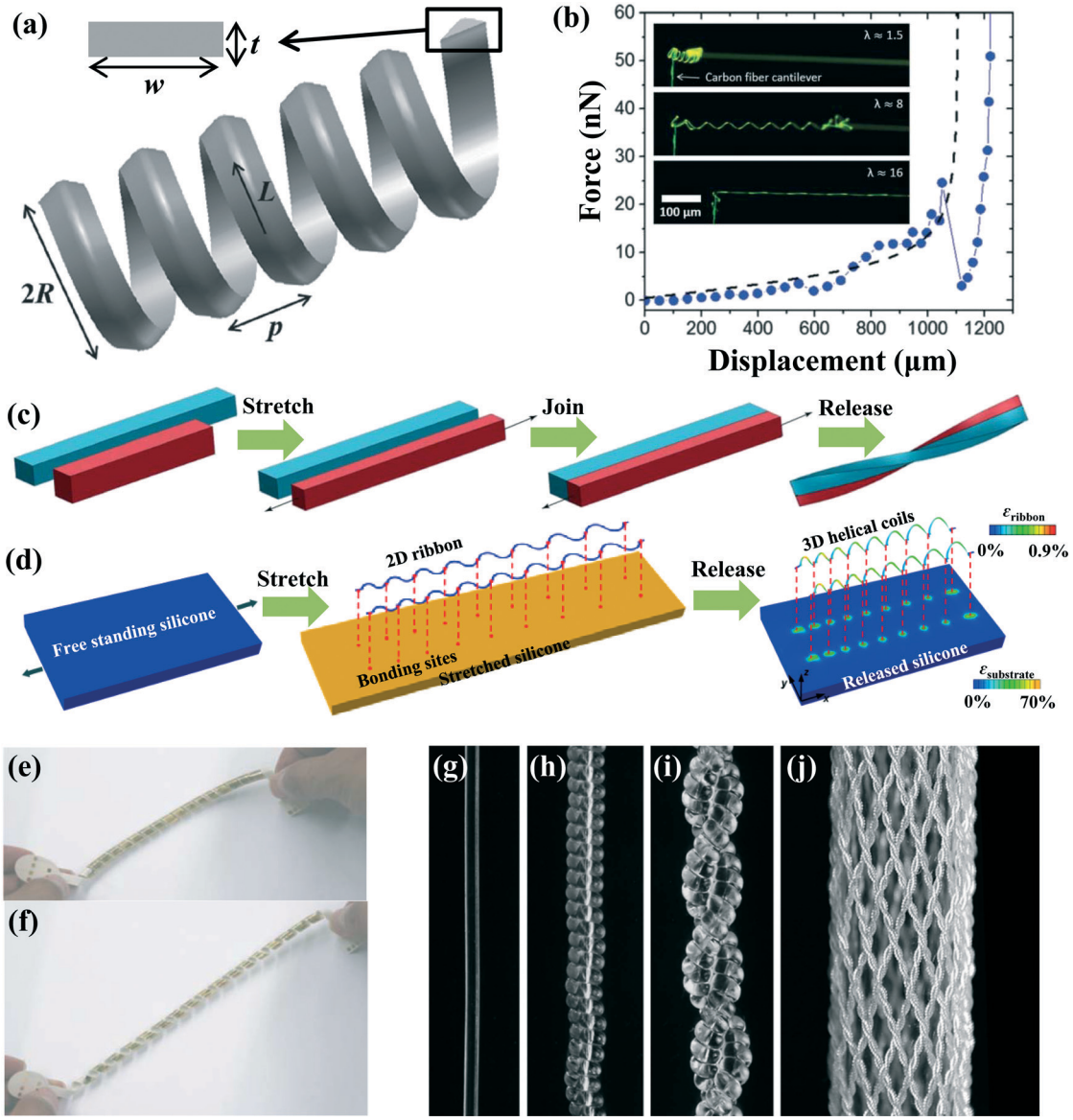

Fig. 5 Helical design. (a) Geometrical illustration of the helical microstructure. (b) Optical image of the stretching process for a helical carbon fiber and its 'J-shaped' stress–strain behavior. (c and d) Two alternative approaches to assembly of the 3D helix from 2D structures. (e and f) A thin-film transistor array helix (e) before and (f) after 50% stretching. (g) A 300 mm-diameter nylon 6,6 fiber; (h) a coil fiber; (i) a two-ply fiber formed from (h); (j) a braid formed from 32 two-ply fiber (i). Panels (a) and (b) are adapted with permission from ref. 105 (Copyright 2014, Royal Society of Chemistry). Panel (c) is adapted with permission from ref. 110 (Copyright 2014, Public Library of Science). Panel (d) is adapted with permission from ref. 112 (Copyright 2015, the American Association for the Advancement of Science). Panels (e) and (f) are adapted with permission from ref. 117 (Copyright 2010, Nature Publishing Group). Panels (g–j) are adapted with permission from ref. 120 (Copyright 2014, the American Association for the Advancement of Science).

quantitatively using a finite-deformation model.[113] Similar processes can form coiled nanowires.[114–116]

By exploiting the compliant nature of the helical structure under small tensile strain, Sekitani *et al.*[117] fabricated a thin-film transistor array on a shape-memory polymer film that was transformed into a helical configuration to shield the electronics from high strains. Fig. 5e and f show this helical thin-film transistor array before and after 50% stretching. To mimic the 'J-shaped' stress–strain behavior of the muscle,[118,119] Haines *et al.*[120] proposed a type of artificial muscle by using the nylon 6,6 coil fibers shown in Fig. 5g–j.

5. Kirigami and origami designs

Kirigami[56,121–124] is an ancient art of paper cutting and folding to form 3D sculptures. Fig. 6a shows a kirigami model in Kent paper (thickness of 0.2–0.3 mm and modulus of 2.45–3.27 GPa) with regularly arranged cuts ($w \simeq 10$–30 mm and $d \simeq 1$–5 mm), and its force–displacement curve is presented in Fig. 6b.[125] In the initial regime (small applied strain), the elementary plates in Kent paper deform mainly *via* in-plane buckling, which leads to a linear force–displacement curve as shown in the inset. As the applied strain

increases (second regime), out-of-plane buckling occurs, resulting in force reduction of the paper. In the final regime, the elementary plates in Kent paper are straightened, which induces an increase in the stiffness again. In this design, a small thickness[126] promotes out-of-plane buckling, and thereby shortens the initial regime. Bahamon *et al.*[127,128] used molecular dynamics (MD) to calculate the stress–strain curve of kirigami structures in graphene, in which the initial stiff regime almost disappears entirely.

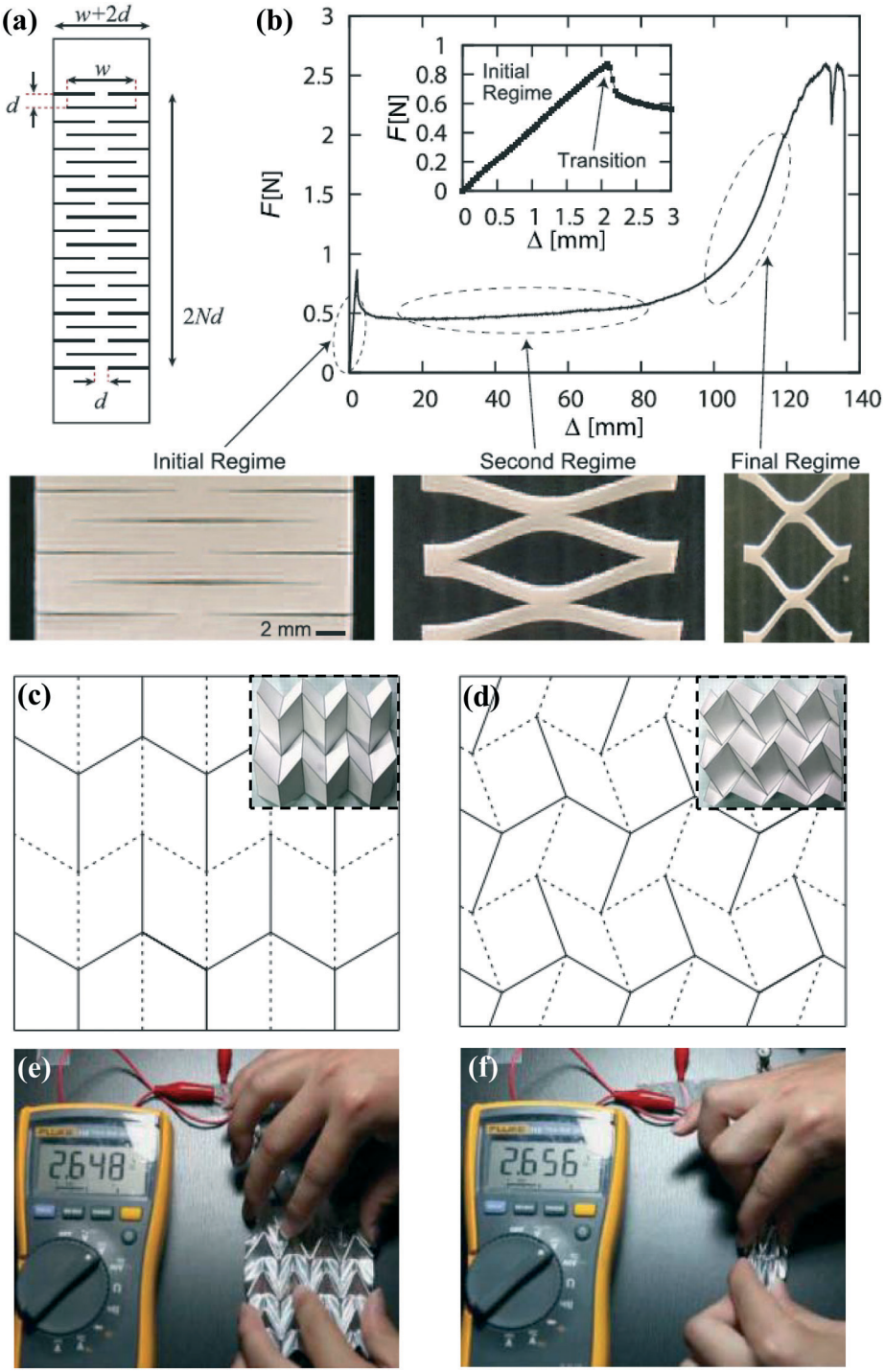

Fig. 6 Kirigami and origami designs. (a) Kirigami pattern in a Kent paper and (b) its force–displacement curve with initial (inset), second and final regimes. Crease mesh and folding morphology for (c) Miura and (d) double corrugation origami. (e) Folding and (f) unfolding status of an origami lithium-ion battery while it was connected to a voltmeter. Panels (a) and (b) are adapted with permission from ref. 125 (Copyright 2016, Nature Publishing Group). Panels (c) and (d) are adapted with permission from ref. 134 (Copyright 2016, The Royal Society). Panels (e) and (f) are adapted with permission from ref. 57 (Copyright 2014, Nature Publishing Group).

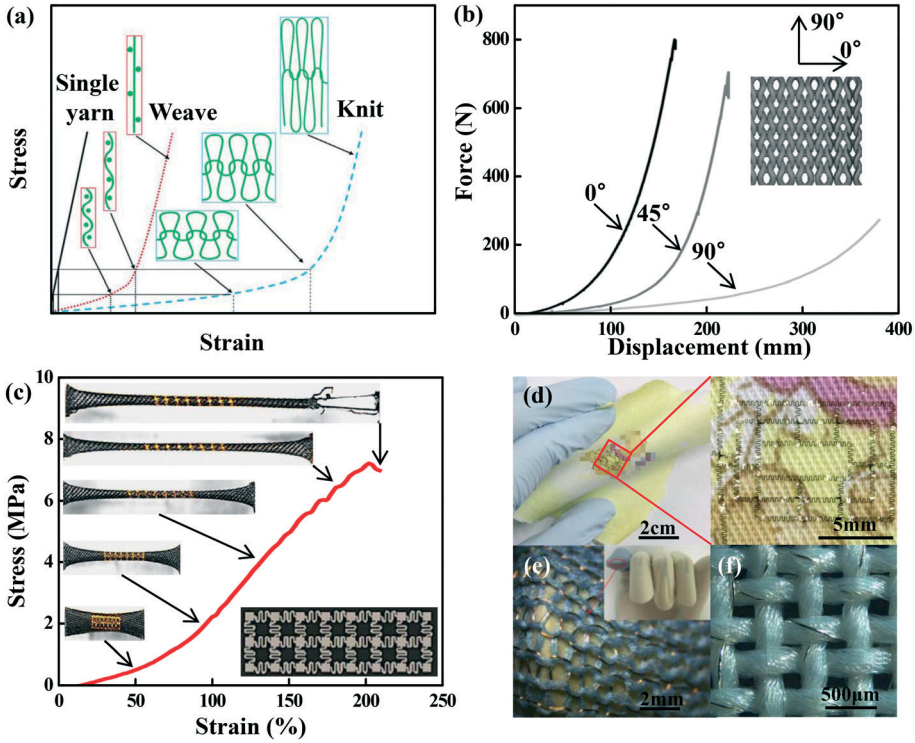

Fig. 7 Textile design. (a) Stress–strain responses of a single yarn, a woven fabric, and a knitted fabric. (b) Anisotropy of a knitted fabric cut under different angles. (c) Stress–strain response of a fabric integrated with stretchable electronics. (d) An ultrathin IGZO-based 7-stage ring oscillator transferred on a handkerchief. (e) A knitted fabric circuit board on a human finger. (f) Copper wires embedded in yarns to realize a textile circuit. Panel (a) is adapted with permission from ref. 58 (Copyright 2017, the American Association for the Advancement of Science). Panel (b) is adapted with permission from ref. 137 (Estonian Academy Publishers). Panel (c) is adapted with permission from ref. 139 (Copyright 2014, Nature Publishing Group). Panel (d) is adapted with permission from ref. 141 (Copyright 2016, Nature Publishing Group). Panel (e) is adapted with permission from ref. 142 (Copyright 2014, The Royal Society). Panel (f) is adapted with permission from ref. 59 (Copyright 2014, MDPI).

Origami[129–133] is an ancient art of paper folding, in which the key is to form pre-defined crease patterns. Fig. 6c and d[134] show two quadrilateral mesh creases. Folding these 'mountain' (solid line) and 'valley' (dotted line) creases forms Miura and double corrugation origami (Fig. 6c and d, inset). These origami designs possess similar mechanics properties as those of the wavy and wrinkled structures. At a small applied strain, the parallelogram faces experience almost zero strains except at the creases, and the entire system has very low stiffness. As the applied strain increases, the folding creases straighten, and the parallelogram faces dominate the stretching such that the structure becomes stiff. These deformation mechanisms result in 'J-shaped' stress–strain behavior.[135] Recently, Yan *et al.*[136] proposed a strategy to produce engineered folding creases for microscale origami structures in polymer films, with 'J-shaped' stress–strain behaviors. Song *et al.*[57] exploited an origami design with 45° Miura folding for application in a lithium-ion battery that is highly deformable at different modes (*e.g.*, stretching, folding, bending and twisting). Fig. 6e and f show folded and unfolded origami

Table 1 Minimum microstructure dimensions, fabrication methods and featured performances of various structural designs to achieve 'J-shaped' stress–strain behaviors

Design	Minimum microstructure dimension	Fabrication	Featured performance
Random network design	~10 nm	Ionic liquid grinding,[63,64] two-step shearing,[65] plasma-induced modification,[66] and two-step polymerization[67]	Small dimension (nano scale)
Deterministic network design	~100 μm	Lithographic approach[49]	High degree of design flexibility
Wavy and wrinkled design	~100 μm	Thermally induced mismatch,[91] pre-strain[92–95]	Sharp transition point, and high ratio of tangent to elastic modulus
Helical design	~10 μm	3D printing,[99] mechanically-guided approach[112]	Strain limiting feature only along the axial direction of helices
Kirigami and origami designs	~10 μm	Lithographic approach,[56] laser cutting,[122] mechanically-guided approach[136]	Transformable between 2D and 3D configurations
Textile design	~1 mm	Weaving,[58] knitting,[58] and braiding[59]	Mature technology for commercial application

lithium-ion batteries where the output voltages remain almost unchanged (2.65 V) during the deformations.

6. Textile design

Textiles are flexible materials that consist of networks of natural or artificial yarns, as shown in Fig. 1f. Weaving and knitting[58] are the most widely used methods for manufacturing textiles. In the weaving process (Fig. 1f, left), perpendicular and individual yarns (warp and weft yarns) interlace together to form the fabric. In the knitting process (Fig. 1f, middle), the yarns adopt wavy, looped configurations, with the potential to offer large stretchabilities. Fig. 7a shows a schematic diagram of stress–strain responses for a single yarn, a woven fabric, and a knitted fabric.[58] The single yarn has a relatively linear stress–strain behavior and a large initial modulus. The 'J-shaped' stress–strain behavior of the knitted fabric is more significant than that of the woven fabric, while they both approach the stiffness of the single yarn at high strain. Fig. 7b shows the load–displacement curves for samples of cotton knitted fabrics cut at different angles,[137] displaying significant anisotropy. The sample cut at the 90° direction has the lowest initial stiffness and largest transition strain between low and high stiffness, followed by the 45° and 0° directions. For 3D textile fabrics, braiding (Fig. 1f, right) is a widely used method, which forms the textile by inter-plaiting yarns along three orthogonal directions, also with capabilities in offering 'J-shaped' stress–strain behavior.[138] Fig. 7c shows stress–strain responses and optical images of a fabric integrated with electronics under stretching.[139] As for the other cases mentioned previously, the 'J-shaped' stress–strain behavior of the fabric maintains compliance of stretchable electronics at small strain, and also eliminates the possibility of failure at large strain.[140]

The rough textures of the fabric can create challenges in the transfer of stretchable electronics onto its surface. Yoon *et al.*[141] introduced an artificial cilia structure at the periphery regions of stretchable electronic platforms as an adhesive element to facilitate transfer printing. Using this strategy, an ultrathin layer of indium gallium zinc oxide as the basis of a 7-stage ring oscillator was successfully transferred onto a handkerchief, as shown in Fig. 7d. Fig. 7e and f show two alternative approaches for integrating stretchable electronics with fabrics: (1) replacing parts of fabric yarns by a metal wire (Fig. 7e);[142] (2) embedding a metal wire into fabric yarns (Fig. 7f).[59]

7. Concluding remarks

Collectively, the advances in materials and mechanics described here provide several promising engineering approaches to materials with 'J-shaped' stress–strain behaviors, with potential for applications in tissue engineering and biomedical devices. Table 1 summarizes the characteristic dimensions, fabrication methods and featured performances of the approaches described in this review paper. Nevertheless, there are many opportunities for further work. For example, previous studies on artificial tissues mainly focus on matching the 'J-shaped' stress–strain responses of biological tissues in 1D (*e.g.*, muscle fiber and ligament), 2D (*e.g.*, skin) or very simple 3D (*e.g.*, trachea and blood vessel) configurations. Reproduction of nonlinear, multi-axial mechanical behaviors in complex 3D organs/tissues remains a challenge. Many biological tissues (*e.g.*, ligament) have intrinsic anisotropic mechanical properties and different tension-compression moduli, also representing design challenges in tissue engineering. In addition to mechanical compatibility with biological tissues, biocompatibility to avoid immune responses in tissue engineering is important to consider, which limits the material selections for the artificial tissues. The strain-limiting structures introduced in this paper offer only a capacity to shield stretchable electronics from in-plane tension. Development of structural designs with strain-limiting properties under in-plane compression or out-of-plane pressure by exploiting 3D designs represents an important direction for future research. Furthermore, the thickness and stiffness of the stretchable electronics increase after integration with the strain-limiting structures, which may increase the foreign body sensation of the biological tissues when wearing such stretchable electronics. Optimization of the structural designs to enable reduced thickness and stiffness of the entire integrated device system is an important consideration for future bio-integrated applications. In conclusion, the above opportunities provide strong motivation for continued and expanded efforts in the fields of biomedical devices and stretchable electronics.

Acknowledgements

Y. M. and X. F. acknowledge the support from the National Basic Research Program of China (Grant No. 2015CB351900) and the National Natural Science Foundation of China (Grant No. 11402135 and 11320101001). Y. Z. acknowledges the support from the National Natural Science Foundation of China (Grant No. 11502129). Y. H. acknowledges the support from NSF (Grant No. DMR-1121262, CMMI-1300846, CMMI-1400169 and CMMI-1534120) and the NIH (Grant No. R01EB019337).

References

1 K. I. Jang, H. N. Jung, J. W. Lee, S. Xu, Y. H. Liu, Y. J. Ma, J. W. Jeong, Y. M. Song, J. Kim, B. H. Kim, A. Badea, J. W. Kwak, Y. Y. Yang, D. W. Shi, Z. Wei, X. Feng, U. Paik, Y. Huang, R. Ghaffari and J. A. Rogers, *Adv. Funct. Mater.*, 2016, **26**, 7281–7290.

2 W. Gao, S. Emaminejad, H. Y. Y. Nyein, S. Challa, K. V. Chen, A. Peck, H. M. Fahad, H. Ota, H. Shiraki, D. Kiriya, D. H. Lien, G. A. Brooks, R. W. Davis and A. Javey, *Nature*, 2016, **529**, 509–514.

3 S. H. Jeong, A. Hagman, K. Hjort, M. Jobs, J. Sundqvist and Z. G. Wu, *Lab Chip*, 2012, **12**, 4657–4664.

4 S. Cheng and Z. G. Wu, *Lab Chip*, 2012, **12**, 2782–2791.
5 B. Y. Ahn, E. B. Duoss, M. J. Motala, X. Y. Guo, S. I. Park, Y. J. Xiong, J. Yoon, R. G. Nuzzo, J. A. Rogers and J. A. Lewis, *Science*, 2009, **323**, 1590–1593.
6 C. Y. Yan and P. S. Lee, *Small*, 2014, **10**, 3443–3460.
7 J. Vanfleteren, M. Gonzalez, F. Bossuyt, Y. Y. Hsu, T. Vervust, I. De Wolf and M. Jablonski, *MRS Bull.*, 2012, **37**, 254–260.
8 B. Huyghe, H. Rogier, J. Vanfleteren and F. Axisa, *IEEE Trans. Adv. Packag.*, 2008, **31**, 802–808.
9 J. Kim, M. Lee, H. J. Shim, R. Ghaffari, H. R. Cho, D. Son, Y. H. Jung, M. Soh, C. Choi, S. Jung, K. Chu, D. Jeon, S. T. Lee, J. H. Kim, S. H. Choi, T. Hyeon and D. H. Kim, *Nat. Commun.*, 2014, **5**, 5747.
10 A. Chortos, J. Liu and Z. A. Bao, *Nat. Mater.*, 2016, **15**, 937–950.
11 J. T. Muth, D. M. Vogt, R. L. Truby, Y. Menguc, D. B. Kolesky, R. J. Wood and J. A. Lewis, *Adv. Mater.*, 2014, **26**, 6307–6312.
12 A. P. Gerratt, H. O. Michaud and S. P. Lacour, *Adv. Funct. Mater.*, 2015, **25**, 2287–2295.
13 C. Pang, J. H. Koo, A. Nguyen, J. M. Caves, M. G. Kim, A. Chortos, K. Kim, P. J. Wang, J. B. H. Tok and Z. A. Bao, *Adv. Mater.*, 2015, **27**, 634–640.
14 H. C. Ko, M. P. Stoykovich, J. Z. Song, V. Malyarchuk, W. M. Choi, C. J. Yu, J. B. Geddes, J. L. Xiao, S. D. Wang, Y. G. Huang and J. A. Rogers, *Nature*, 2008, **454**, 748–753.
15 Y. M. Song, Y. Z. Xie, V. Malyarchuk, J. L. Xiao, I. Jung, K. J. Choi, Z. J. Liu, H. Park, C. F. Lu, R. H. Kim, R. Li, K. B. Crozier, Y. G. Huang and J. A. Rogers, *Nature*, 2013, **497**, 95–99.
16 D. Rus and M. T. Tolley, *Nature*, 2015, **521**, 467–475.
17 N. S. Lu and D. H. Kim, *Soft Robotics*, 2014, **1**, 53–62.
18 D. H. Kim, N. S. Lu, R. Ma, Y. S. Kim, R. H. Kim, S. D. Wang, J. Wu, S. M. Won, H. Tao, A. Islam, K. J. Yu, T. I. Kim, R. Chowdhury, M. Ying, L. Z. Xu, M. Li, H. J. Chung, H. Keum, M. McCormick, P. Liu, Y. W. Zhang, F. G. Omenetto, Y. G. Huang, T. Coleman and J. A. Rogers, *Science*, 2011, **333**, 838–843.
19 R. C. Webb, Y. Ma, S. Krishnan, Y. Li, S. Yoon, X. Guo, X. Feng, Y. Shi, M. Seidel, N. H. Cho, J. Kurniawan, J. Ahad, N. Sheth, J. Kim, J. G. Taylor VI, T. Darlington, K. Chang, W. Huang, J. Ayers, A. Gruebele, R. M. Pielak, M. J. Slepian, Y. Huang, A. M. Gorbach and J. A. Rogers, *Sci. Adv.*, 2015, **1**, e1500701.
20 S. J. Benight, C. Wang, J. B. H. Tok and Z. A. Bao, *Prog. Polym. Sci.*, 2013, **38**, 1961–1977.
21 T. Someya, T. Sekitani, S. Iba, Y. Kato, H. Kawaguchi and T. Sakurai, *Proc. Natl. Acad. Sci. U. S. A.*, 2004, **101**, 9966–9970.
22 D. Son, J. Lee, S. Qiao, R. Ghaffari, J. Kim, J. E. Lee, C. Song, S. J. Kim, D. J. Lee, S. W. Jun, S. Yang, M. Park, J. Shin, K. Do, M. Lee, K. Kang, C. S. Hwang, N. S. Lu, T. Hyeon and D. H. Kim, *Nat. Nanotechnol.*, 2014, **9**, 397–404.
23 S. Xu, Y. H. Zhang, L. Jia, K. E. Mathewson, K. I. Jang, J. Kim, H. R. Fu, X. Huang, P. Chava, R. H. Wang, S. Bhole, L. Z. Wang, Y. J. Na, Y. Guan, M. Flavin, Z. S. Han, Y. G. Huang and J. A. Rogers, *Science*, 2014, **344**, 70–74.
24 S. X. Yang, Y. C. Chen, L. Nicolini, P. Pasupathy, J. Sacks, B. Su, R. Yang, D. Sanchez, Y. F. Chang, P. L. Wang, D. Schnyer, D. Neikirk and N. S. Lu, *Adv. Mater.*, 2015, **27**, 6423–6430.
25 L. Z. Xu, S. R. Gutbrod, Y. J. Ma, A. Petrossians, Y. H. Liu, R. C. Webb, J. A. Fan, Z. J. Yang, R. X. Xu, J. J. Whalen, J. D. Weiland, Y. G. Huang, I. R. Efimov and J. A. Rogers, *Adv. Mater.*, 2015, **27**, 1731–1737.
26 B. W. Lu, Y. Chen, D. P. Ou, H. Chen, L. W. Diao, W. Zhang, J. Zheng, W. G. Ma, L. Z. Sun and X. Feng, *Sci. Rep.*, 2015, **5**, 16065.
27 I. R. Minev, P. Musienko, A. Hirsch, Q. Barraud, N. Wenger, E. M. Moraud, J. Gandar, M. Capogrosso, T. Milekovic, L. Asboth, R. F. Torres, N. Vachicouras, Q. H. Liu, N. Pavlova, S. Duis, A. Larmagnac, J. Voros, S. Micera, Z. G. Suo, G. Courtine and S. P. Lacour, *Science*, 2015, **347**, 159–163.
28 S. P. Lacour, G. Courtine and J. Guck, *Nat. Rev. Mater.*, 2016, **1**, 16063.
29 W. Yang, V. R. Sherman, B. Gludovatz, E. Schaible, P. Stewart, R. O. Ritchie and M. A. Meyers, *Nat. Commun.*, 2015, **6**, 6649.
30 S. J. Ling, Q. Zhang, D. L. Kaplan, F. Omenetto, M. J. Buehler and Z. Qin, *Lab Chip*, 2016, **16**, 2459–2466.
31 A. L. Kwansa, Y. M. Empson, E. C. Ekwueme, V. I. Walters, J. W. Freeman and C. T. Laurencin, *Soft Matter*, 2010, **6**, 5016–5025.
32 M. A. Meyers, J. McKittrick and P. Y. Chen, *Science*, 2013, **339**, 773–779.
33 S. W. Cranford, A. Tarakanova, N. M. Pugno and M. J. Buehler, *Nature*, 2012, **482**, 72–76.
34 P. Chamiot-Clerc, X. Copie, J. F. Renaud, M. Safar and X. Girerd, *Cardiovasc. Res.*, 1998, **37**, 811–819.
35 M. E. Safar, J. Blacher, J. J. Mourad and G. M. London, *Stroke*, 2000, **31**, 782–790.
36 G. A. Holzapfel, *Biomechanics of soft tissue*, 2001, Academic Press, pp. 1049–1063.
37 C. H. Lee, Y. J. Ma, K. I. Jang, A. Banks, T. Pan, X. Feng, J. S. Kim, D. Kang, M. S. Raj, B. L. McGrane, B. Morey, X. Y. Wang, R. Ghaffari, Y. G. Huang and J. A. Rogers, *Adv. Funct. Mater.*, 2015, **25**, 3698–3704.
38 Y. Ma, M. Pharr, L. Wang, J. Kim, Y. Liu, Y. Xue, R. Ning, X. Wang, H. U. Chung, X. Feng, J. A. Rogers and Y. Huang, *Small*, 2017, **13**, 1602954.
39 Y. J. Ma, K. I. Jang, L. Wang, H. N. Jung, J. W. Kwak, Y. G. Xue, H. Chen, Y. Y. Yang, D. W. Shi, X. Feng, J. A. Rogers and Y. G. Huang, *Adv. Funct. Mater.*, 2016, **26**, 5345–5351.
40 Y. H. Zhang, S. D. Wang, X. T. Li, J. A. Fan, S. Xu, Y. M. Song, K. J. Choi, W. H. Yeo, W. Lee, S. N. Nazaar, B. W. Lu, L. Yin, K. C. Hwang, J. A. Rogers and Y. G. Huang, *Adv. Funct. Mater.*, 2014, **24**, 2028–2037.
41 A. Robinson, A. Aziz, Q. Liu, Z. Suo and S. P. Lacour, *J. Appl. Phys.*, 2014, **115**, 143511.
42 A. Romeo, Q. H. Liu, Z. G. Suo and S. P. Lacour, *Appl. Phys. Lett.*, 2013, **102**, 131904.
43 J. A. Rogers, T. Someya and Y. G. Huang, *Science*, 2010, **327**, 1603–1607.
44 D. H. Kim, N. S. Lu, Y. G. Huang and J. A. Rogers, *MRS Bull.*, 2012, **37**, 226–235.

45 Y. H. Zhang, Y. G. Huang and J. A. Rogers, *Curr. Opin. Solid State Mater. Sci.*, 2015, **19**, 190–199.
46 N. S. Lu and S. X. Yang, *Curr. Opin. Solid State Mater. Sci.*, 2015, **19**, 149–159.
47 M. Gonzalez, F. Axisa, M. V. BuIcke, D. Brosteaux, B. Vandevelde and J. Vanfleteren, *Microelectron. Reliab.*, 2008, **48**, 825–832.
48 S. Choi, H. Lee, R. Ghaffari, T. Hyeon and D. H. Kim, *Adv. Mater.*, 2016, **28**, 4203–4218.
49 K. I. Jang, H. U. Chung, S. Xu, C. H. Lee, H. W. Luan, J. Jeong, H. Y. Cheng, G. T. Kim, S. Y. Han, J. W. Lee, J. Kim, M. Cho, F. X. Miao, Y. Y. Yang, H. N. Jung, M. Flavin, H. Liu, G. W. Kong, K. J. Yu, S. I. Rhee, J. Chung, B. Kim, J. W. Kwak, M. H. Yun, J. Y. Kim, Y. M. Song, U. Paik, Y. H. Zhang, Y. Huang and J. A. Rogers, *Nat. Commun.*, 2015, **6**, 6566.
50 D. Y. Khang, H. Q. Jiang, Y. Huang and J. A. Rogers, *Science*, 2006, **311**, 208–212.
51 Y. G. Sun, W. M. Choi, H. Q. Jiang, Y. G. Y. Huang and J. A. Rogers, *Nat. Nanotechnol.*, 2006, **1**, 201–207.
52 H. J. Bae, S. Bae, C. Park, S. Han, J. Kim, L. N. Kim, K. Kim, S. H. Song, W. Park and S. Kwon, *Adv. Mater.*, 2015, **27**, 2083–2089.
53 W. M. Choi, J. Z. Song, D. Y. Khang, H. Q. Jiang, Y. Y. Huang and J. A. Rogers, *Nano Lett.*, 2007, **7**, 1655–1663.
54 S. J. Gerbode, J. R. Puzey, A. G. McCormick and L. Mahadevan, *Science*, 2012, **337**, 1087–1091.
55 P. N. Chen, Y. F. Xu, S. S. He, X. M. Sun, S. W. Pan, J. Deng, D. Y. Chen and H. S. Peng, *Nat. Nanotechnol.*, 2015, **10**, 1077–1083.
56 T. C. Shyu, P. F. Damasceno, P. M. Dodd, A. Lamoureux, L. Z. Xu, M. Shlian, M. Shtein, S. C. Glotzer and N. A. Kotov, *Nat. Mater.*, 2015, **14**, 785–789.
57 Z. M. Song, T. Ma, R. Tang, Q. Cheng, X. Wang, D. Krishnaraju, R. Panat, C. K. Chan, H. Y. Yu and H. Q. Jiang, *Nat. Commun.*, 2014, **5**, 3140.
58 A. Maziz, A. Concas, A. Khaldi, J. Stalhand, N. K. Persson and E. W. H. Jager, *Sci. Adv.*, 2017, **3**, e1600327.
59 M. Stoppa and A. Chiolerio, *Sensors*, 2014, **14**, 11957–11992.
60 A. J. Licup, S. Munster, A. Sharma, M. Sheinman, L. M. Jawerth, B. Fabry, D. A. Weitz and F. C. MacKintosh, *Proc. Natl. Acad. Sci. U. S. A.*, 2015, **112**, 9573–9578.
61 T. van Dillen, P. R. Onck and E. Van der Giessen, *J. Mech. Phys. Solids*, 2008, **56**, 2240–2264.
62 P. R. Onck, T. Koeman, T. van Dillen and E. van der Giessen, *Phys. Rev. Lett.*, 2005, **95**, 178102.
63 T. Sekitani, Y. Noguchi, K. Hata, T. Fukushima, T. Aida and T. Someya, *Science*, 2008, **321**, 1468–1472.
64 S. S. Yao and Y. Zhu, *Adv. Mater.*, 2015, **27**, 1480–1511.
65 Y. J. Ma, X. F. Yao, Q. S. Zheng, Y. J. Yin, D. J. Jiang, G. H. Xu, F. Wei and Q. Zhang, *Appl. Phys. Lett.*, 2010, **97**, 061909.
66 R. R. Wang, H. T. Zhai, T. Wang, X. Wang, Y. Cheng, L. J. Shi and J. Sun, *Nano Res.*, 2016, **9**, 2138–2148.
67 Q. Chen, H. Chen, L. Zhu and J. Zheng, *J. Mater. Chem. B*, 2015, **3**, 3654–3676.
68 E. Ban, V. H. Barocas, M. S. Shephard and C. R. Picu, *J. Appl. Mech.*, 2016, **83**, 041008.
69 P. Jungebluth, J. C. Haag, S. Sjoqvist, Y. Gustafsson, A. B. Rodriguez, C. Del Gaudio, A. Bianco, I. Dehnisch, P. Uhlen, S. Baiguera, G. Lemon, M. L. Lim and P. Macchiarini, *Nat. Protoc.*, 2014, **9**, 2164–2179.
70 P. Lee, J. Lee, H. Lee, J. Yeo, S. Hong, K. H. Nam, D. Lee, S. S. Lee and S. H. Ko, *Adv. Mater.*, 2012, **24**, 3326–3332.
71 J. J. Liang, L. Li, K. Tong, Z. Ren, W. Hu, X. F. Niu, Y. S. Chen and Q. B. Pei, *ACS Nano*, 2014, **8**, 1590–1600.
72 H. Le Ferrand, S. Bolisetty, A. F. Demirors, R. Libanori, A. R. Studart and R. Mezzenga, *Nat. Commun.*, 2016, **7**, 12078.
73 S. De, P. J. King, P. E. Lyons, U. Khan and J. N. Coleman, *ACS Nano*, 2010, **4**, 7064–7072.
74 C. Gao, S. Zhang, F. Wang, B. Wen, C. Han, Y. Ding and M. Yang, *ACS Appl. Mater. Interfaces*, 2014, **6**, 12252–12260.
75 M. P. Garrett, I. N. Ivanov, R. A. Gerhardt, A. A. Puretzky and D. B. Geohegan, *Appl. Phys. Lett.*, 2010, **97**, 163105.
76 L. Hu, D. S. Hecht and G. Gruner, *Nano Lett.*, 2004, **4**, 2513–2517.
77 N. A. Fleck and X. M. Qiu, *J. Mech. Phys. Solids*, 2007, **55**, 562–588.
78 S. H. Kang, S. Shan, A. Kosmrlj, W. L. Noorduin, S. Shian, J. C. Weaver, D. R. Clarke and K. Bertoldi, *Phys. Rev. Lett.*, 2014, **112**, 098701.
79 L. R. Meza, S. Das and J. R. Greer, *Science*, 2014, **345**, 1322–1326.
80 L. R. Meza, A. J. Zelhofer, N. Clarke, A. J. Mateos, D. M. Kochmann and J. R. Greer, *Proc. Natl. Acad. Sci. U. S. A.*, 2015, **112**, 11502–11507.
81 J. Liu, T. Y. Gu, S. C. Shan, S. H. Kang, J. C. Weaver and K. Bertoldi, *Adv. Mater.*, 2016, **28**, 6619–6624.
82 Y. K. Lee, K. I. Jang, Y. J. Ma, A. Koh, H. Chen, H. N. Jung, Y. Kim, J. W. Kwak, L. Wang, Y. G. Xue, Y. Y. Yang, W. L. Tian, Y. Jiang, Y. H. Zhang, X. Feng, Y. G. Huang and J. A. Rogers, *Adv. Funct. Mater.*, 2017, **27**, 1605476.
83 M. Arslan and M. C. Boyce, *J. Appl. Mech.*, 2006, **73**, 536–543.
84 Y. H. Zhang, S. Xu, H. R. Fu, J. Lee, J. Su, K. C. Hwang, J. A. Rogers and Y. G. Huang, *Soft Matter*, 2013, **9**, 8062–8070.
85 Y. H. Zhang, H. R. Fu, Y. W. Su, S. Xu, H. Y. Cheng, J. A. Fan, K. C. Hwang, J. A. Rogers and Y. G. Huang, *Acta Mater.*, 2013, **61**, 7816–7827.
86 G. Lanzara, N. Salowitz, Z. Q. Guo and F. K. Chang, *Adv. Mater.*, 2010, **22**, 4643–4648.
87 D. H. Kim, J. Z. Song, W. M. Choi, H. S. Kim, R. H. Kim, Z. J. Liu, Y. Y. Huang, K. C. Hwang, Y. W. Zhang and J. A. Rogers, *Proc. Natl. Acad. Sci. U. S. A.*, 2008, **105**, 18675–18680.
88 Y. A. Huang, Y. Z. Wang, L. Xiao, H. M. Liu, W. T. Dong and Z. P. Yin, *Lab Chip*, 2014, **14**, 4205–4212.
89 Q. Ma, H. Y. Cheng, K. I. Jang, H. W. Luan, K. C. Hwang, J. A. Rogers, Y. G. Huang and Y. H. Zhang, *J. Mech. Phys. Solids*, 2016, **90**, 179–202.
90 Q. Ma and Y. H. Zhang, *J. Appl. Mech.*, 2016, **83**, 111008.

91 N. Bowden, S. Brittain, A. G. Evans, J. W. Hutchinson and G. M. Whitesides, *Nature*, 1998, **393**, 146–149.
92 J. Jones, S. P. Lacour, S. Wagner and Z. G. Suo, *J. Vac. Sci. Technol., A*, 2004, **22**, 1723–1725.
93 H. Q. Jiang, D. Y. Khang, J. Z. Song, Y. G. Sun, Y. G. Huang and J. A. Rogers, *Proc. Natl. Acad. Sci. U. S. A.*, 2007, **104**, 15607–15612.
94 F. Xu, X. Wang, Y. T. Zhu and Y. Zhu, *Adv. Funct. Mater.*, 2012, **22**, 1279–1283.
95 Y. Zhu and F. Xu, *Adv. Mater.*, 2012, **24**, 1073–1077.
96 Y. J. Ma, Y. G. Xue, K. I. Jang, X. Feng, J. A. Rogers and Y. Huang, *Proc. R. Soc. London, Ser. A*, 2016, **472**, 20160339.
97 M. Kaltenbrunner, T. Sekitani, J. Reeder, T. Yokota, K. Kuribara, T. Tokuhara, M. Drack, R. Schwodiauer, I. Graz, S. Bauer-Gogonea, S. Bauer and T. Someya, *Nature*, 2013, **499**, 458–463.
98 D. H. Kim, J. H. Ahn, W. M. Choi, H. S. Kim, T. H. Kim, J. Z. Song, Y. G. Y. Huang, Z. J. Liu, C. Lu and J. A. Rogers, *Science*, 2008, **320**, 507–511.
99 R. D. Farahani, K. Chizari and D. Therriault, *Nanoscale*, 2014, **6**, 10470–10485.
100 E. L. Starostin and G. H. M. van der Heijden, *J. Mech. Phys. Solids*, 2009, **57**, 959–969.
101 J. T. Pham, J. Lawrence, D. Y. Lee, G. M. Grason, T. Emrick and A. J. Crosby, *Adv. Mater.*, 2013, **25**, 6703–6708.
102 B. Q. Jia, L. Yu, F. Y. Fu, L. Y. Li, J. P. Zhou and L. N. Zhang, *RSC Adv.*, 2014, **4**, 9112–9117.
103 H. Wada and R. R. Netz, *Europhys. Lett.*, 2007, **77**, 68001.
104 J. W. Freeman, M. D. Woods and C. T. Laurencin, *J. Biomech.*, 2007, **40**, 2029–2036.
105 J. T. Pham, J. Lawrence, G. M. Grason, T. Emrick and A. J. Crosby, *Phys. Chem. Chem. Phys.*, 2014, **16**, 10261–10266.
106 A. Yamada, F. Niikura and K. Ikuta, *J. Micromech. Microeng.*, 2008, **18**, 025035.
107 L. L. Lebel, B. Aissa, M. A. El Khakani and D. Therriault, *Adv. Mater.*, 2010, **22**, 592–596.
108 S. Z. Guo, F. Gosselin, N. Guerin, A. M. Lanouette, M. C. Heuzey and D. Therriault, *Small*, 2013, **9**, 4118–4122.
109 J. S. Huang, J. Liu, B. Kroll, K. Bertoldi and D. R. Clarke, *Soft Matter*, 2012, **8**, 6291–6300.
110 J. Liu, J. S. Huang, T. X. Su, K. Bertoldi and D. R. Clarke, *PLoS One*, 2014, **9**, 98183.
111 T. Savin, N. A. Kurpios, A. E. Shyer, P. Florescu, H. Y. Liang, L. Mahadevan and C. J. Tabin, *Nature*, 2011, **476**, 57–62.
112 S. Xu, Z. Yan, K. I. Jang, W. Huang, H. R. Fu, J. Kim, Z. Wei, M. Flavin, J. McCracken, R. Wang, A. Badea, Y. Liu, D. Q. Xiao, G. Y. Zhou, J. Lee, H. U. Chung, H. Y. Cheng, W. Ren, A. Banks, X. L. Li, U. Paik, R. G. Nuzzo, Y. G. Huang, Y. H. Zhang and J. A. Rogers, *Science*, 2015, **347**, 154–159.
113 Y. Liu, Z. Yan, Q. Lin, X. L. Guo, M. D. Han, K. Nan, K. C. Hwang, Y. G. Huang, Y. H. Zhang and J. A. Rogers, *Adv. Funct. Mater.*, 2016, **26**, 2909–2918.
114 Y. L. Chen, Y. Zhu, X. Chen and Y. L. Liu, *J. Appl. Mech.*, 2016, **83**, 041011.
115 F. Xu, W. Lu and Y. Zhu, *ACS Nano*, 2011, **5**, 672–678.
116 Y. L. Chen, Y. L. Liu, Y. Yan, Y. Zhu and X. Chen, *J. Mech. Phys. Solids*, 2016, **95**, 25–43.
117 T. Sekitani, U. Zschieschang, H. Klauk and T. Someya, *Nat. Mater.*, 2010, **9**, 1015–1022.
118 A. E. Toscano, K. M. Ferraz, R. M. de Castro and F. Canon, *Clinics*, 2010, **65**, 1363–1369.
119 G. M. Odegard, T. L. Haut Donahue, D. A. Morrow and K. R. Kaufman, *J. Biomech. Eng.*, 2008, **130**, 061017.
120 C. S. Haines, M. D. Lima, N. Li, G. M. Spinks, J. Foroughi, J. D. W. Madden, S. H. Kim, S. L. Fang, M. J. de Andrade, F. Goktepe, O. Goktepe, S. M. Mirvakili, S. Naficy, X. Lepro, J. Y. Oh, M. E. Kozlov, S. J. Kim, X. R. Xu, B. J. Swedlove, G. G. Wallace and R. H. Baughman, *Science*, 2014, **343**, 868–872.
121 M. K. Blees, A. W. Barnard, P. A. Rose, S. P. Roberts, K. L. McGill, P. Y. Huang, A. R. Ruyack, J. W. Kevek, B. Kobrin, D. A. Muller and P. L. McEuen, *Nature*, 2015, **524**, 204–207.
122 A. Lamoureux, K. Lee, M. Shlian, S. R. Forrest and M. Shtein, *Nat. Commun.*, 2015, **6**, 8092.
123 Y. H. Zhang, Z. Yan, K. W. Nan, D. Q. Xiao, Y. H. Liu, H. W. Luan, H. R. Fu, X. Z. Wang, Q. L. Yang, J. C. Wang, W. Ren, H. Z. Si, F. Liu, L. H. Yang, H. J. Li, J. T. Wang, X. L. Guo, H. Y. Luo, L. Wang, Y. G. Huang and J. A. Rogers, *Proc. Natl. Acad. Sci. U. S. A.*, 2015, **112**, 11757–11764.
124 Z. M. Song, X. Wang, C. Lv, Y. H. An, M. B. Liang, T. Ma, D. He, Y. J. Zheng, S. Q. Huang, H. Y. Yu and H. Q. Jiang, *Sci. Rep.*, 2015, **5**, 10988.
125 M. Isobe and K. Okumura, *Sci. Rep.*, 2016, **6**, 24758.
126 R. X. Xu, K. I. Jang, Y. J. Ma, H. N. Jung, Y. Y. Yang, M. Cho, Y. H. Zhang, Y. Huang and J. A. Rogers, *Extreme Mech. Lett.*, 2014, **1**, 120–126.
127 D. A. Bahamon, Z. N. Qi, H. S. Park, V. M. Pereira and D. K. Campbell, *Phys. Rev. B*, 2016, **93**, 235408.
128 Z. N. Qi, D. K. Campbell and H. S. Park, *Phys. Rev. B*, 2014, **90**, 245437.
129 L. H. Dudte, E. Vouga, T. Tachi and L. Mahadevan, *Nat. Mater.*, 2016, **15**, 583–588.
130 J. L. Silverberg, J. H. Na, A. A. Evans, B. Liu, T. C. Hull, C. D. Santangelo, R. J. Lang, R. C. Hayward and I. Cohen, *Nat. Mater.*, 2015, **14**, 389–393.
131 S. S. Tolman, I. L. Delimont, L. L. Howell and D. T. Fullwood, *Smart Mater. Struct.*, 2014, **23**, 094010.
132 E. T. Filipov, T. Tachi and G. H. Paulino, *Proc. Natl. Acad. Sci. U. S. A.*, 2015, **112**, 12321–12326.
133 R. Tang, H. Huang, H. E. Tu, H. S. Liang, M. B. Liang, Z. M. Song, Y. Xu, H. Q. Jiang and H. Y. Yu, *Appl. Phys. Lett.*, 2014, **104**, 083501.
134 K. Saito, A. Tsukahara and Y. Okabe, *Proc. R. Soc. London, Ser. A*, 2016, **472**, 20150235.
135 E. T. Filipov, G. H. Paulino and T. Tachi, *Proc. R. Soc. London, Ser. A*, 2016, **472**, 20150607.
136 Z. Yan, F. Zhang, J. C. Wang, F. Liu, X. L. Guo, K. W. Nan, Q. Lin, M. Y. Gao, D. Q. Xiao, Y. Shi, Y. T. Qiu, H. W. Luan, J. H. Kim, Y. Q. Wang, H. Y. Luo, M. D. Han, Y. G. Huang,

Y. H. Zhang and J. A. Rogers, *Adv. Funct. Mater.*, 2016, **26**, 2629–2639.

137 O. Kononova, A. Krasnikovs, K. Dzelzitis, G. Kharkova, A. Vagel and M. Eiduks, *Est. J. Eng.*, 2011, **17**, 39–50.

138 L. Heller, D. Vokoun, P. Sittner and H. Finckh, *Smart Mater. Struct.*, 2012, **21**, 045016.

139 K. I. Jang, S. Y. Han, S. Xu, K. E. Mathewson, Y. H. Zhang, J. W. Jeong, G. T. Kim, C. Webb, J. W. Lee, T. J. Dawidczyk, R. H. Kim, Y. M. Song, W. H. Yeo, S. Kim, H. Y. Cheng, S. Il Rhee, J. Chung, B. Kim, H. U. Chung, D. J. Lee, Y. Y. Yang, M. Cho, J. G. Gaspar, R. Carbonari, M. Fabiani, G. Gratton, Y. G. Huang and J. A. Rogers, *Nat. Commun.*, 2014, **5**, 4779.

140 D. H. Kim, Y. S. Kim, J. Wu, Z. Liu, J. Song, H. S. Kim, Y. Huang, K. C. Hwang and J. Rogers, *Adv. Mater.*, 2009, **21**, 3703–3707.

141 J. Yoon, Y. Jeong, H. Kim, S. Yoo, H. S. Jung, Y. Kim, Y. Hwang, Y. Hyun, W. K. Hong, B. H. Lee, S. H. Choa and H. C. Ko, *Nat. Commun.*, 2016, **7**, 11477.

142 Q. Li and X. M. Tao, *Proc. R. Soc. London, Ser. A*, 2014, **470**, 20140472.

